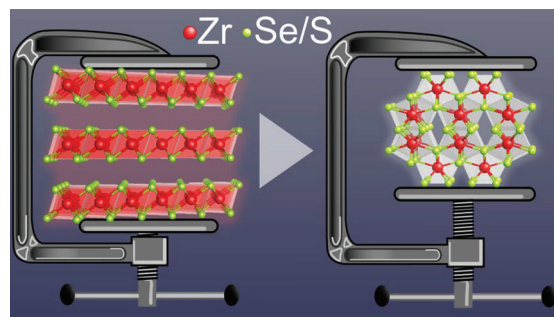


Structural Phase Transition and Bandgap Control through Mechanical Deformation in Layered Semiconductors 1T–ZrX₂ (X = S, Se)

Edoardo Martino,^{*} David Santos-Cottin, Florian Le Mardelé, Konstantin Semeniuk, Michele Pizzochero, Kristiāns Čerņevičs, Benoît Baptiste, Ludovic Delbes, Stefan Klotz, Francesco Capitani, Helmuth Berger, Oleg V. Yazyev, and Ana Akrap^{*}

ABSTRACT: Applying elastic deformation can tune a material's physical properties locally and reversibly. Spatially modulated lattice deformation can create a bandgap gradient, favoring photogenerated charge separation and collection in optoelectronic devices. These advantages are hindered by the maximum elastic strain that a material can withstand before breaking. Nanomaterials derived by exfoliating transition metal dichalcogenides (TMDs) are an ideal playground for elastic deformation, as they can sustain large elastic strains, up to a few percent. However, exfoliable TMDs with highly strain-tunable properties have proven challenging for researchers to identify. We investigated 1T-ZrS₂ and 1T-ZrSe₂, exfoliable semiconductors with large bandgaps. Under compressive deformation, both TMDs dramatically change their physical properties. 1T-ZrSe₂ undergoes a reversible transformation into an exotic three-dimensional lattice, with a semiconductor-to-metal transition. In ZrS₂, the irreversible transformation between two different layered structures is accompanied by a sudden 14% bandgap reduction. These results establish that Zr-based TMDs are an optimal strain-tunable platform for spatially textured bandgaps, with a strong potential for novel optoelectronic devices and light harvesting.



When developing semiconductor-based devices for photovoltaic, photocatalytic, or photosensing applications, light harvesting efficiencies can be optimized by fine-tuning the size or even the spatial variation of the electronic bandgap. This can be achieved by mechanical actions, such as strain or hydrostatic pressure. Application of high pressure is an experimentally accessible path for exploring how the properties of a material change upon varying the interatomic distances.¹

Established techniques, such as X-ray diffraction (XRD), can then be used in combination to thoroughly quantify the response of crystalline systems to various mechanical actions and compute the corresponding compressibility and elastic moduli.

Once a material's mechanical and electronic response to applied forces is known, one can design a device in which, for example, a specific strain induced in the photosensitive component attunes it to a chosen wavelength. A variety of tools and methods for such strain-tuning have been implemented and reported, such as local compression by AFM cantilevers,² adhesion to an elastomeric substrate,^{3,4} patterned substrates,^{5,6} differential thermal expansion between

the active material and the substrate,⁷ and the use of active piezoelectric actuators⁸ or microelectromechanical systems.⁹

Layered van der Waals materials are especially good candidates for strain-engineered optoelectronic devices,^{10–12} thanks to their proven extremely wide range of elastic strain, which they can support (above 5%), when reduced to nanometer thickness by exfoliation.¹³ The strain tuning of optoelectronic properties of layered materials, such as transition metal dichalcogenides (TMDs), has already been proposed and successfully demonstrated for the semiconducting compounds containing group 6 metals: 2H-MoS₂ and 2H-WSe₂.^{14–16} Furthermore, tuning the bandgap in TMDs by mechanical action has been used to enhance the performance of semiconducting devices for light harvesting applications.¹⁷

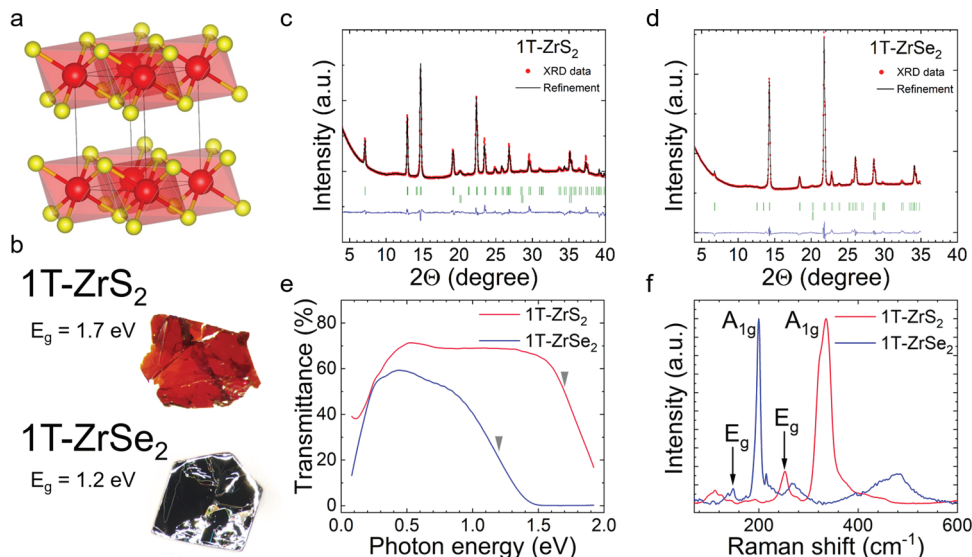


Figure 1. Structural and optical properties of 1T-ZrS₂ and 1T-ZrSe₂. (a) Crystal structure of both ZrS₂ and ZrSe₂. Red and yellow spheres represent the metal and chalcogen atoms, respectively. The octahedra formed by the chalcogens around the central Zr atom are shown. (b) Photographs of the single crystals used for the experiments. The bright red color of ZrS₂ is the result of its optical bandgap in the visible range. (c, d) Rietveld-refined powder X-ray diffraction (XRD) of 1T-ZrS₂ and 1T-ZrSe₂ measured at low pressure (< 1 GPa) inside the diamond anvil cell. Red dots are the experimental data, and the black lines are the simulated patterns for the known crystal structures. The diffraction pattern from the steel gasket is also included into the refinement. (e) Optical transmittance through thin samples (6 and 2 μ m for ZrS₂ and ZrSe₂, respectively), where the arrows indicate the positions of the indirect bandgaps at the onset of optical absorption. (f) Raman spectra with the indexed A_{1g} and E_g phonon modes, shared by both materials due to their identical crystalline symmetry. Raman active modes are in ZrS₂, $A_{1g} = 334$ cm⁻¹ and $E_g = 249$ cm⁻¹; in ZrSe₂, $A_{1g} = 195$ cm⁻¹ and $E_g = 146$ cm⁻¹.

The prototypical 2H-MoS₂ and 2H-WSe₂ are, however, not the only semiconducting layered TMDs. These also include systems with group 4 metals, such as Zr and Hf. The corresponding bandgaps range from 1.2 to 2 eV, pertinent for optoelectronic and energy conversion applications. These compounds have so far been neglected in comparison to the Mo- and W-based semiconductors, despite their rather promising properties, which encompass a high electronic mobility¹⁸ and a tendency to spontaneously form native oxides with high dielectric constant.¹⁹ The salient differences between group 4 and group 6 TMDs are in the electronic energy bands' orbital character.²⁰ Group 4 TMDs have two fewer valence electrons on the metal atom, and a different metal-chalcogen coordination. Group 6 compounds, for example MoS₂, crystallize in the 2H polytype, where the metal is in a trigonal prismatic coordination with six chalcogen atoms. Both conduction and valence bands have a metallic, d orbital character, giving the chalcogen a minor role in the electronic structure. In contrast, Zr- and Hf-based TMDs assume the 1T-polytype structure with a six-fold octahedral metal-chalcogen coordination. Their conduction bands originate from the transition metal d orbitals, while the chalcogen p orbitals are responsible for the valence bands.

Realizing a structural phase transition driven by applying a mechanical action is a long-standing desire of the community working on layered semiconductors, such as TMDs. A mechanically induced lattice reconstruction in TMDs can open a venue for strain-controlled semiconductor-to-metal conversion.²¹ This phenomenon can be utilized in tunable optoelectronic elements or in clean metal-semiconductor lateral homojunctions,^{22,23} operated by a stretchable substrate. However, for 2H-MoS₂ and 2H-WSe₂, it is not possible to mechanically induce phase transition that involves in-plane reorganization, like a transformation from a 2H into a 1T

phase. In fact, structural changes in these compounds cannot be triggered by strain or pressure alone^{24–27} and additionally require high temperatures, laser irradiation, or intercalation.^{28,29} In the present study, we investigated 1T-ZrS₂ and 1T-ZrSe₂, motivated by the 1T polytypes being considerably more prone to structural instabilities than the 2H polytypes. In light of the different chalcogen size for the investigated materials, Se being larger than S, their response under applied pressure may be expected to vary. For both mentioned compounds, we observed transitions between two distinct crystalline structures, characterized by different electronic properties. Such lattice reconstructions commonly occur in metallic TMDs and are responsible for the unusual transport properties of 1T-TaS₂³⁰ and topological phase transitions in 1T-MoTe₂.³¹ The transition temperatures at which these transformations manifest can be tuned in a broad temperature range by applied pressure.^{32–34} Indeed, by means of ab initio calculations, Zhai et al.,³⁵ predicted a structural phase transition to occur in 1T-ZrS₂ at high pressure. To test this experimentally in 1T-ZrS₂ and 1T-ZrSe₂, we measured their optical and structural properties under quasi-hydrostatic pressure that we applied using a diamond anvil cell.

Figure 1 summarizes a set of structural, infrared and Raman properties for 1T-ZrS₂ and 1T-ZrSe₂ at ambient pressure. The data were recorded on the same samples as those later used for the high-pressure experiments, and are consistent with the published results.³⁷ Optical transmission measurements (Figure 1e) show transparency in a wide energy range, and the onset of optical absorption at the indirect bandgap energies, which are 1.7 eV for ZrS₂ and 1.2 eV for ZrSe₂. Transparency in the infrared range is accompanied by a remarkably high room-temperature dc conductivity, measured using a standard 4-point technique, of 3.13 S/cm (0.31 Ω cm) for ZrS₂, and 23.81 S/cm (0.04 Ω cm) for ZrSe₂. The high

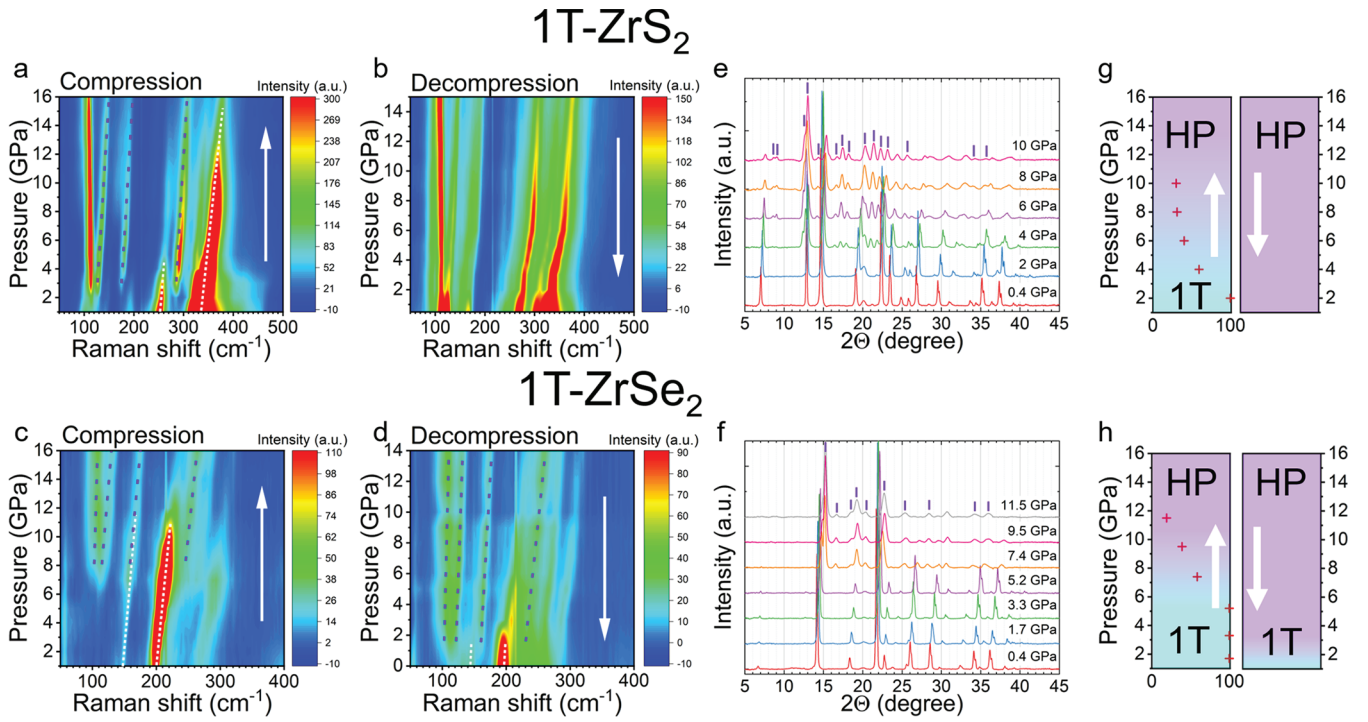


Figure 2. Evidence of pressure-induced structural phase transitions (a, b) Raman spectra of ZrS_2 during compression (a) and decompression (b). The dotted white and purple lines are guides for the eyes in the low- and high-pressure phases, respectively. The compression curve shows the onset of transformation at 3 GPa. During decompression the high-pressure phase remains stable down to 1 atm. (c, d) Pressure evolution of the Raman spectra of ZrSe_2 . Data during compression (c) shows the appearance of a new crystalline phase at 8 GPa, and the initial phase is restored during decompression below 2 GPa (d). (e, f) Powder X-ray diffraction at different pressures for ZrS_2 (e) and ZrSe_2 (f). The purple lines mark the diffraction peaks originating from the new crystalline phase. (g, h) Schematic representation of the pressure driven transformation. The blue and purple regions represent the ambient-pressure and high-pressure phases, respectively. The red crosses show the volume fraction of the 1T phase as a function of pressure during compression.

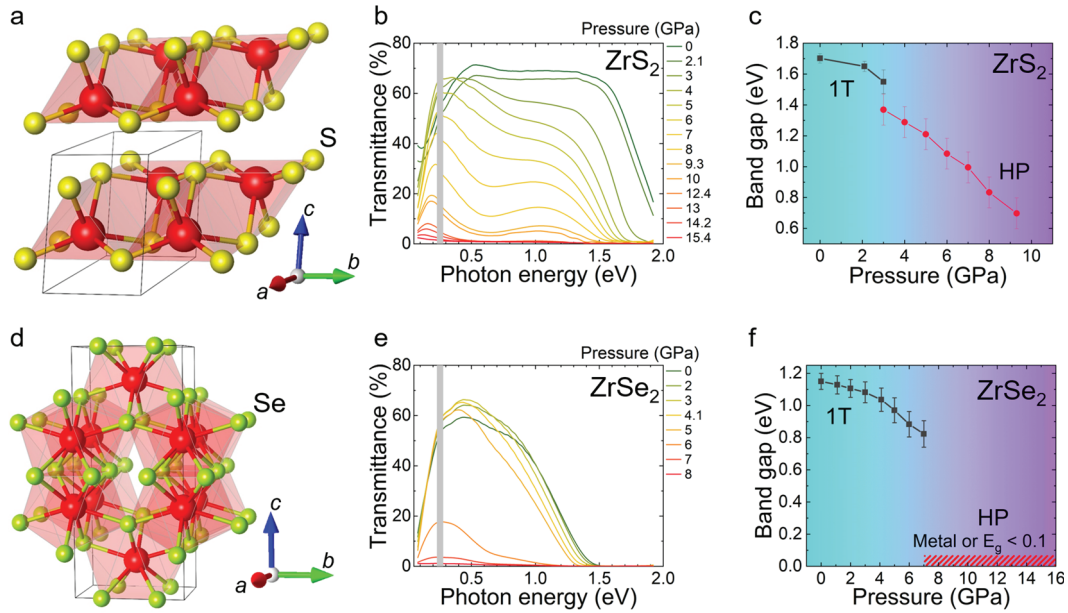


Figure 3. High-pressure structures and switching of optical properties. (a) Crystal structure of HP-ZrS_2 . The layered structure is evident, while the original octahedral coordination is distorted into an unusual trigonal prismatic configuration. (b) Optical transmittance as a function of pressure for ZrS_2 . (c) ZrS_2 bandgap evolution under pressure. (d) Crystal structure of HP-ZrSe_2 . The atomic lattice is three-dimensional, a rare configuration that exists at ambient pressure in ErSe_2 and UTe_2 . (e) Optical transmittance measured up to 8 GPa. As the new phase appears, optical transmittance becomes zero due to its metallic properties. (f) ZrSe_2 bandgap evolution under pressure. The grey area in the panels b and e are the 0.23–0.28 eV region obscured by diamond absorption.

intrinsic doping level of these materials,^{36,37} causing their high dc conductivity, is also evidenced by the intense light absorbance at low energies (<0.5 eV). This is most likely due to in-gap or shallow donor states.

Single crystals of Zr-based TMDs were loaded into a diamond anvil cell for optical measurements under high-pressure conditions. A finely ground powder was used for X-ray diffraction experiments. The applied pressure was monitored using ruby fluorescence.³⁸ The compressive strain imposed onto the materials at every specific pressure was calculated from our data, and can be found in the SI. The pressure dependence of the Raman and powder XRD patterns are shown in Figure 2. For both materials, the formations of different crystalline structures are evident from the appearance of new peaks in the Raman and XRD spectra. In ZrS₂, the new crystalline phase starts to appear at 3 GPa, which corresponds to 1% in-plane compression and 4% out-of-plane compression (Figure SI.3). With increasing pressure, a larger fraction of the sample is converted into this new phase, with the low- and high-pressure phases coexisting over a broad range of pressures. The transformation into the newly created phase, here called HP-ZrS₂, is irreversible upon full decompression to 1 atm. ZrSe₂ remains structurally stable up to 8 GPa, equivalent to 3% in-plane compression and 7% out-of-plane compression (Figure SI.3). Upon further increase of pressure, a structural transformation takes place, with a more rapid conversion of the material compared to the S-based compound. The high-pressure phase (HP-ZrSe₂) persists down to 2 GPa when pressure is released. Below 2 GPa, the initial structure is recovered, making the transformation reversible, but with a wide hysteresis. The progression and reversibility of the phase transitions as a function of pressure are schematically depicted in Figure 2g and h. The different behaviour between the two isostructural materials—different transformation onset pressures as well as the presence or absence of reversibility—suggests a possible difference in the crystalline structure of the high-pressure phases. It is not yet clear what makes this structural transformation favorable only for these specific types of TMDs, but we believe that the different metal-chalcogen coordination, when compared to 2H-polytypes, and the fact that there are two fewer valence electrons²⁰ on the transition metal, must play a fundamental role.

Using our high-pressure XRD and Raman data and aided by the work of Zhai et al.,³⁵ we succeeded in refining the crystalline structures of HP-ZrS₂ and HP-ZrSe₂. For ZrS₂, mechanical deformation transforms the known layered material into a new layered structure (Figure 3a), previously never observed in a TMD. The octahedra are transformed into distorted trigonal prisms. The structure is different from that of a 2H phase, as the triangular bases of the prisms are now parallel to the *bc*-plane, and their orientation alternates in the *a*-axis direction. Even more surprising and unusual is the structure assumed by ZrSe₂. This initially layered material becomes three-dimensional, a transformation that is reminiscent of the graphite to diamond conversion. The resultant crystalline structure—orthorhombic with the space group *Immm*—is unusual and can be observed at ambient conditions only in exotic materials, such as the rare-earth dichalcogenide ErSe₂³⁹ and the unconventional heavy-Fermion superconductor UTe₂.⁴⁰ The Zr atoms are coordinated by 8 chalcogens, a configuration that can also be found at ambient pressure in the quasi-one-dimensional crystals ZrS₃ and ZrSe₃.⁴¹

Rietveld refinement of the powder X-ray diffraction patterns was done for every pressure point (Figures SI.1 and 2). This was used to determine the possible crystal structure for the high-pressure phases, along with the compressibility and volume fraction of the 1T phase as a function of pressure.

Having identified the crystalline structures, the optical and electronic properties of those newly created materials are of immediate interest. By measuring optical transmittance as a function of pressure, we investigated the presence and magnitude of the optical bandgap (further details can be found in the SI). For ZrS₂, at low pressures (0 to 2 GPa) the bandgap of the 1T phase is reduced, like it is commonly seen in other TMDs.^{24,25} Above 3 GPa, as the new phase appears, it is possible to identify the contribution to absorption from a second bandgap, which is approximately 200 meV smaller than that of the native 1T phase. As pressure further increases, the bandgap decreases, offering additional control over the optical properties. At the same time, the volume ratio between the two phases changes, as seen from the XRD data (SI), further modifying the optical spectrum. To confirm our estimate of the optical bandgap, we performed first-principle calculations on the ZrS₂ HP phase at 6 GPa. The computed band structure has an optical bandgap of 1 eV, in perfect agreement with the value extracted from the experimental data (Figure SI.8). The origin of a small suppression of optical transmittance in the 0.5–1 eV energy range remains unclear.

ZrSe₂ changes its properties more dramatically. We observed a continuous reduction of the bandgap of the 1T phase up to 5 GPa. As the new crystalline phase appears, the optical transparency is suppressed for all frequencies. This means that HP-ZrSe₂ is metallic,⁴² or possibly a narrow-gap semiconductor with a bandgap of less than 0.1 eV. The evolution of the optical bandgaps extracted from the optical transmittance data is summarized in Figure 3c and f.

To further address the dramatic pressure-induced semiconductor-to-metal transition observed in ZrSe₂, the band structure for the proposed high-pressure phase was computed by means of semilocal Perdew–Burke–Ernzerhof⁴³ functional. Specifically, we determined the electronic band structures of both the low-pressure (0 GPa) and the high-pressure (9.5 GPa) phases by means of density functional theory. The low-pressure phase is found to be a semiconductor, with an indirect bandgap of 0.9 eV (see Figure 4a). This value is in agreement with our optical measurements shown in Figure 3e and f, and perfectly matches the results of recent ARPES experiments.³⁶ We found that the valence band maximum is located at the centre of the Brillouin zone, while the conduction band minimum occurs at the high-symmetry L point. As far as the high-pressure phase of ZrSe₂ is concerned, the present optical measurements cannot distinguish whether this system is a metal or a semiconductor with a bandgap below 0.1 eV, which is the lowest energy we could probe with our experimental setup. Our calculations reported in Figure 4b clearly indicate a metallic character, with a number of bands crossing the Fermi level. Overall, our calculations paint a picture in accordance with the experimental observations.

To conclude, we have experimentally demonstrated room-temperature pressure-driven structural phase transitions in the semiconducting layered transition metal dichalcogenides 1T-ZrS₂ and 1T-ZrSe₂. The two materials are isostructural and isoelectronic, but undergo completely different lattice reconstructions, and their physical properties evolve in distinct manners. Under applied pressure of 3 GPa, ZrS₂ is transformed

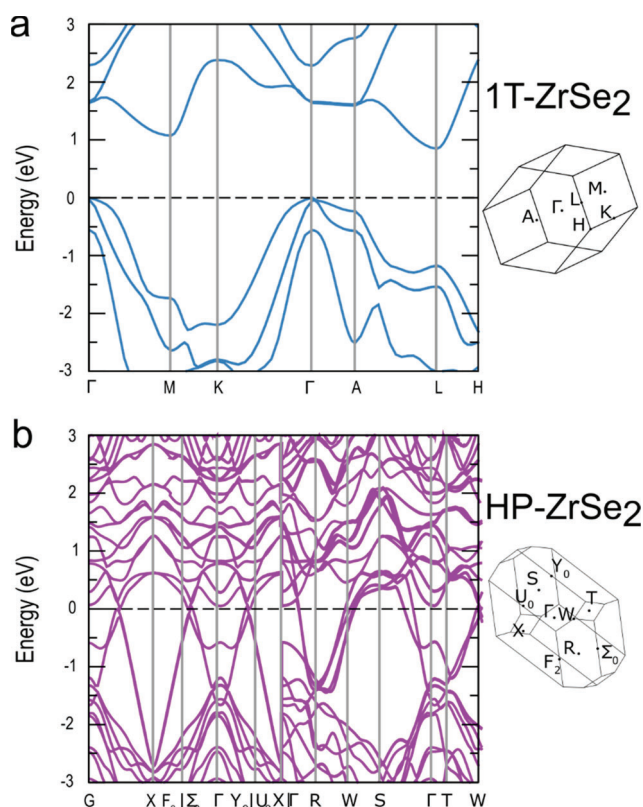


Figure 4. First-principles calculations of the electronic structure of ZrSe_2 . Electronic band structure of the (a) low-pressure and (b) high-pressure crystalline phases of ZrSe_2 , together with the high-symmetry points in the corresponding first Brillouin zones.

irreversibly into a new layered structure, with a consequent reduction of the bandgap by 200 meV. As for ZrSe_2 , once pressure is above 8 GPa, the layers merge into a 3D structure. This collapse results in a semiconductor-to-metal transition, as confirmed by ab initio calculations. In addition, the bandgap of the starting 1T phase reduces under compression at the rate of 50 meV/GPa, giving a further tunability over the materials' optical properties. Our demonstration of structural transformations induced by mechanical actions, with the associated dramatic changes in their electronic properties, grants the long-awaited additional functionality in TMDs, enabling us to control structure and properties on-demand. New opportunities in the field of strain-designed devices—charge funneling and clean metal–semiconductor homojunctions in optoelectronic components—are now within reach. Further research needs to be done in the direction of understanding the dynamics of the lattice reconstruction, in particular for ZrSe_2 because of its close reminiscence to the graphite to diamond transformation.

■ ASSOCIATED CONTENT

SI Supporting Information

The Supporting Information is available free of charge at <https://pubs.acs.org/doi/10.1021/acsmaterialslett.0c00252>.

Experimental details including crystal synthesis, high-pressure Raman and infrared spectroscopy, X-ray diffraction, and density functional theory calculations, high-pressure Rietveld refinement of the XRD spectra, pressure–strain relation, high-pressure Raman scatter-

ing, band gap estimation from optical transmittance, and DFT band structure calculations (PDF)

■ AUTHOR INFORMATION

Corresponding Authors

Edoardo Martino — Institute of Physics, Ecole Polytechnique Fédérale de Lausanne (EPFL), CH-1015 Lausanne, Switzerland; orcid.org/0000-0001-9654-9820; Email: edoardo.martino@epfl.ch

Ana Akrap — Department of Physics, University of Fribourg, CH-1700 Fribourg, Switzerland; Email: ana.akrap@unifr.ch

Authors

David Santos-Cottin — Department of Physics, University of Fribourg, CH-1700 Fribourg, Switzerland

Florian Le Mardelé — Department of Physics, University of Fribourg, CH-1700 Fribourg, Switzerland

Konstantin Semeniuk — Institute of Physics, Ecole Polytechnique Fédérale de Lausanne (EPFL), CH-1015 Lausanne, Switzerland

Michele Pizzochero — Institute of Physics, Ecole Polytechnique Fédérale de Lausanne (EPFL), CH-1015 Lausanne, Switzerland; orcid.org/0000-0003-3948-8202

Kristīans Čerņevičs — Institute of Physics, Ecole Polytechnique Fédérale de Lausanne (EPFL), CH-1015 Lausanne, Switzerland

Benoît Baptiste — Institut de Minéralogie, de Physique des Matériaux et de Cosmochimie, Sorbonne University, CNRS UMR 7590, IMPMC, F-75005 Paris, France

Ludovic Delbes — Institut de Minéralogie, de Physique des Matériaux et de Cosmochimie, Sorbonne University, CNRS UMR 7590, IMPMC, F-75005 Paris, France

Stefan Klotz — Institut de Minéralogie, de Physique des Matériaux et de Cosmochimie, Sorbonne University, CNRS UMR 7590, IMPMC, F-75005 Paris, France

Francesco Capitani — Synchrotron-SOLEIL, F-91192 Gif-sur-Yvette Cedex, France; orcid.org/0000-0003-1161-7455

Helmuth Berger — Institute of Physics, Ecole Polytechnique Fédérale de Lausanne (EPFL), CH-1015 Lausanne, Switzerland

Oleg V. Yazyev — Institute of Physics, Ecole Polytechnique Fédérale de Lausanne (EPFL), CH-1015 Lausanne, Switzerland; orcid.org/0000-0001-7281-3199

Complete contact information is available at: <https://pubs.acs.org/doi/10.1021/acsmaterialslett.0c00252>

Author Contributions

E.M. conceived the project and designed the experiments. H.B. grew the samples. E.M., D.S.C., F.L.M., K.S., and F.C. performed the high-pressure Raman and infrared spectroscopy experiments. S.K., L.D., and B.P. performed the high-pressure X-ray diffraction experiments. D.S.C., E.M., S.K., L.D., and B.P. analyzed and refined the X-ray diffraction patterns. K.C., M.P., and O.V.Y. performed DFT calculations of band structure. A.A. supervised the project. E.M. wrote the paper, and all authors commented on the manuscript.

Notes

The authors declare no competing financial interest. The data that support the findings of this study are available from E.M. and A.A. upon reasonable request.

■ ACKNOWLEDGMENTS

The authors acknowledge illuminating discussions with Laszlo Forró, Nathaniel Miller, Anna Celeste, Ferenc Borodincs, Quansheng Wu, Zoran Rukelj, and Alexey Kuzmenko. We would like to thank Philippe Rosier and Nicolas Dumesnil (from IMPMC) for the production of mechanical parts which were useful for mounting the diamond anvil cell on the diffractometer and high-pressure X-ray diffraction experiments. E.M. and K.S. acknowledge funding from the Swiss National Science Foundation through its SINERGIA network MPBH and Grant 200021_175836. A.A. acknowledges funding from the Swiss National Science Foundation through Project PP00P2_170544. M.P., K.C., and O.V.Y. are financially supported by the Swiss National Science Foundation through the Grant 172543. First-principles calculations were performed at the Swiss National Supercomputing Centre (CSCS) under the Project s832. Experiment at Synchrotron Soleil was supported by the Grant Proposal ID 20190927.

■ REFERENCES

- (1) Willardson, R.; Weber, E.; Paul, W.; Suski, T. *High Pressure Semiconductor Physics I*; Academic Press, 1998.
- (2) Manzeli, S.; Allain, A.; Ghadimi, A.; Kis, A. Piezoresistivity and strain-induced band gap tuning in atomically thin MoS₂. *Nano Lett.* **2015**, *15*, 5330–5335.
- (3) Castellanos-Gomez, A.; et al. Local strain engineering in atomically thin MoS₂. *Nano Lett.* **2013**, *13*, 5361–5366.
- (4) Zhang, Q.; et al. Strain relaxation of monolayer WS₂ on plastic substrate. *Adv. Funct. Mater.* **2016**, *26*, 8707–8714.
- (5) Levy, N.; et al. Strain-induced pseudo-magnetic fields greater than 300 Tesla in graphene nanobubbles. *Science* **2010**, *329*, 544–547.
- (6) Li, H.; et al. Optoelectronic crystal of artificial atoms in strain-textured molybdenum disulphide. *Nat. Commun.* **2015**, *6*, 7381.
- (7) Frisenda, R.; et al. Biaxial strain tuning of the optical properties of single-layer transition metal dichalcogenides. *npj 2D Mater. Appl.* **2017**, *1*, 10.
- (8) Martín-Sánchez, J.; et al. Strain-tuning of the optical properties of semiconductor nanomaterials by integration onto piezoelectric actuators. *Semicond. Sci. Technol.* **2018**, *33* (1), 013001.
- (9) Christopher, J. W.; et al. Monolayer MoS₂ strained to 1.3% with a microelectromechanical system. *J. Microelectromech. Syst.* **2019**, *28* (2), 254–263.
- (10) Lien, M.-B.; et al. Ranging and light field imaging with transparent photodetectors. *Nat. Photonics* **2020**, *14* (3), 143–148.
- (11) Tong, L.; et al. Stable mid-infrared polarization imaging based on quasi-2D tellurium at room temperature. *Nat. Commun.* **2020**, *11* (1), 2308.
- (12) Liu, S.; et al. Manipulating efficient light emission in two-dimensional perovskite crystals by pressure-induced anisotropic deformation. *Science advances* **2019**, *5* (7), eaav9445.
- (13) Deng, S.; Sumant, A. V.; Berry, V. Strain engineering in two-dimensional nanomaterials beyond graphene. *Nano Today* **2018**, *22*, 14–35.
- (14) Feng, J.; Qian, X.; Huang, C. W.; Li, J. Strain-engineered artificial atom as a broad-spectrum solar energy funnel. *Nat. Photonics* **2012**, *6*, 866–872.
- (15) Xie, S.; et al. Coherent, atomically thin transition-metal dichalcogenide superlattices with engineered strain. *Science* **2018**, *359*, 1131–1136.
- (16) Conley, H. J.; et al. Bandgap engineering of strained monolayer and bilayer MoS₂. *Nano Lett.* **2013**, *13*, 3626–3630.
- (17) De Sanctis, A.; Amit, I.; Heppelstone, S. P.; Craciun, M. F.; Russo, S. Strain-engineered inverse charge-funnelling in layered semiconductors. *Nat. Commun.* **2018**, *9*, 1652.
- (18) Zhang, W.; Huang, Z.; Zhang, W.; Li, Y. Two-dimensional semiconductors with possible high room temperature mobility. *Nano Res.* **2014**, *7*, 1731–1737.
- (19) Lai, S.; et al. HfO₂/HfS₂ hybrid heterostructure fabricated via controllable chemical conversion of two-dimensional HfS₂. *Nanoscale* **2018**, *10*, 18758–18766.
- (20) Kolobov, A. V.; Tominaga, J. Two-Dimensional Transition-Metal Dichalcogenides. *Springer Ser. Mater. Sci.* **2016**, DOI: 10.1007/978-3-319-31450-1.
- (21) Duerloo, K.-A. N.; Li, Y.; Reed, E. J. Structural phase transitions in two-dimensional Mo- and W-dichalcogenide monolayers. *Nat. Commun.* **2014**, *5*, 4214.
- (22) Eda, G.; et al. Coherent atomic and electronic heterostructures of single-layer MoS₂. *ACS Nano* **2012**, *6*, 7311–7317.
- (23) Kappera, R.; et al. Phase-engineered low-resistance contacts for ultrathin MoS₂ transistors. *Nat. Mater.* **2014**, *13*, 1128–1134.
- (24) Nayak, A. P.; et al. Pressure-induced semiconducting to metallic transition in multilayered molybdenum disulphide. *Nat. Commun.* **2014**, *5*, 3731.
- (25) Zhao, Z.; et al. Pressure induced metallization with absence of structural transition in layered molybdenum diselenide. *Nat. Commun.* **2015**, *6*, 7312.
- (26) Wang, X.; et al. Pressure-induced iso-structural phase transition and metallization in WSe₂. *Sci. Rep.* **2017**, *7*, 46694.
- (27) Caramazza, S.; et al. Effect of pressure on optical properties of the transition metal dichalcogenide MoSe₂. *J. Phys.: Conf. Ser.* **2017**, *950*, 042012.
- (28) Guo, Y.; et al. Probing the dynamics of the metallic-to-semiconducting structural phase transformation in MoS₂ crystals. *Nano Lett.* **2015**, *15*, 5081–5088.
- (29) Wang, L.; Xu, Z.; Wang, W.; Bai, X. Atomic mechanism of dynamic electrochemical lithiation processes of MoS₂ nanosheets. *J. Am. Chem. Soc.* **2014**, *136*, 6693–6697.
- (30) Martino, E.; et al. Preferential out-of-plane conduction and quasi-one-dimensional electronic states in layered van der Waals material 1T-TaS₂. *npj 2D Mater. Appl.* **2020**, *4*, 7.
- (31) Wang, Z.; et al. MoTe₂: A type-II Weyl topological metal. *Phys. Rev. Lett.* **2016**, *117* (5), 056805.
- (32) Sipos, B.; et al. From Mott state to superconductivity in 1T-TaS₂. *Nat. Mater.* **2008**, *7*, 960–965.
- (33) Berger, A. N.; et al. Temperature-driven topological transition in 1T'-MoTe₂. *npj Quantum Mater.* **2018**, *3*, 2.
- (34) Heikes, C.; et al. Mechanical control of crystal symmetry and superconductivity in Weyl semimetal MoTe₂. *Phys. Rev. Mater.* **2018**, *2*, 74202.
- (35) Zhai, H.; et al. Pressure-induced phase transition, metallization and superconductivity in ZrS₂. *Phys. Chem. Chem. Phys.* **2018**, *20*, 23656–23663.
- (36) Ghafari, A.; Moustafa, M.; Di Santo, G.; Petaccia, L.; Janowitz, C. Opposite dispersion bands at the Fermi level in ZrSe₂. *Appl. Phys. Lett.* **2018**, *112*, 182105.
- (37) Moustafa, M.; Zandt, T.; Janowitz, C.; Manzke, R. Growth and band gap determination of the ZrS_xSe_{2-x} single crystal series. *Phys. Rev. B: Condens. Matter Mater. Phys.* **2009**, *80*, 035206.
- (38) Mao, H. K.; Bell, P. M.; Shaner, J. W.; Steinberg, D. J. Specific volume measurements of Cu, Mo, Pd, and Ag and calibration of the ruby R1 fluorescence pressure gauge from 0.06 to 1 Mbar. *J. Appl. Phys.* **1978**, *49*, 3276–3283.
- (39) Haase, D. J.; Steinfink, H.; Weiss, E. J. The Phase Equilibria and Crystal Chemistry of the Rare Earth Group VI Systems. I. Erbium-Selenium. *Inorg. Chem.* **1965**, *4*, 538–540.
- (40) Aoki, D. Unconventional Superconductivity in Heavy Fermion UTe₂. *J. Phys. Soc. Jpn.* **2019**, *88*, 043702.
- (41) Furuseth, S.; Brattas, L.; Kjekshus, A.; et al. Crystal Structures of TiS₃, ZrS₃, ZrSe₃, ZrTe₃, HfS₃ and HfSe₃. *Acta Chem. Scand.* **1975**, *29*, 623–631.
- (42) Peter, Y. U.; Cardona, M. *Fundamentals of Semiconductors: Physics and Materials Properties*; Springer Science & Business Media, 2010.
- (43) Perdew, J. P.; Burke, K.; Ernzerhof, M. Generalized gradient approximation made simple. *Phys. Rev. Lett.* **1996**, *77*, 3865–3868.